




RESEARCH PAPER THEMED ISSUE

Pharmacological properties of TRPM3 isoforms are determined by the length of the pore loop

Katharina Held^{1,2,3,4}  | Vincenzo Davide Aloï^{1,2,3} | Ana Cristina Nogueira Freitas^{2,3} | Annelies Janssens^{2,3} | Andrei Segal^{2,3} | Julia Przibilla⁵ | Stephan Ernst Philipp⁵ | Yu Tian Wang⁴ | Thomas Voets^{2,3}  | Joris Vriens¹ 

¹Laboratory of Endometriosis, Endometriosis and Reproductive Medicine, Department of Development and Regeneration, KU Leuven, Leuven, Belgium

²Laboratory of Ion Channel Research, VIB-KU Leuven Center for Brain and Disease Research, Leuven, Belgium

³Department of Molecular Medicine, KU Leuven, Leuven, Belgium

⁴DM Centre for Brain Health, Department of Medicine, University of British Columbia, Vancouver, British Columbia, Canada

⁵Experimental and Clinical Pharmacology and Toxicology/Center for Molecular Signaling (PZMS), Saarland University, Homburg, Germany

Correspondence

Joris Vriens, Laboratory of Endometriosis, Endometriosis and Reproductive Medicine, Department of Development and Regeneration, KU Leuven, Herestraat 49 box 611, Leuven 3000, Belgium.
Email: joris.vriens@kuleuven.be

Funding information

Stichting Tegen Kanker, Grant/Award Number: TRPM3; University Foundation from Belgium, Grant/Award Number: WA-0292; Saarland University (HOMFOR); Belgian Foundation Against Cancer; Queen Elisabeth Medical Foundation for Neurosciences; Research Council of the KU Leuven, Grant/Award Number: C1-TRPLe; Research Foundation-Flanders, Grant/Award Numbers: G.0B1819N, G.084515N, G.0825.11, G.0565.07; Belgian Federal Government, Grant/Award Number: IUAP P7/13

Background and Purpose: Transient receptor potential melastatin 3 (TRPM3) is a non-selective cation channel that plays a pivotal role in the peripheral nervous system as a transducer of painful heat signals. Alternative splicing gives rise to several TRPM3 variants. The functional consequences of these splice isoforms are poorly understood. Here, the pharmacological properties of TRPM3 variants arising from alternative splicing in the pore-forming region were compared.

Experimental Approach: Calcium microfluorimetry and patch clamp recordings were used to compare the properties of heterologously expressed TRPM3 α 1 (long pore variant) and TRPM3 α 2- α 6 (short pore variants). Furthermore, site-directed mutagenesis was done to investigate the influence of the length of the pore loop on the channel function.

Key Results: All short pore loop TRPM3 α variants (TRPM3 α 2- α 6) were activated by the neurosteroid pregnenolone sulphate (PS) and by nifedipine, whereas the long pore loop variant TRPM3 α 1 was insensitive to either compound. In contrast, TRPM3 α 1 was robustly activated by clotrimazole, a compound that does not directly activate the short pore variants but potentiates their responses to PS. Clotrimazole-activated TRPM3 α 1 currents were largely insensitive to established TRPM3 α 2 antagonists and were only partially inhibited upon activation of the μ opioid receptor. Finally, by creating a set of mutant channels with pore loops of intermediate length, we showed that the length of the pore loop dictates differential channel activation by PS and clotrimazole.

Conclusion and Implications: Alternative splicing in the pore-forming region of TRPM3 defines the channel's pharmacological properties, which depend critically on the length of the pore-forming loop.

Abbreviations: Clt, clotrimazole; DRG, dorsal root ganglion; HEK293, human embryonic kidney 293; HTS, hypotonic solution; Nif, nifedipine; PS, pregnenolone sulphate; TRP, transient receptor potential; TRPM3, transient receptor potential melastatin 3.

This is an open access article under the terms of the Creative Commons Attribution-NonCommercial License, which permits use, distribution and reproduction in any medium, provided the original work is properly cited and is not used for commercial purposes.

© 2020 The Authors. British Journal of Pharmacology published by John Wiley & Sons Ltd on behalf of British Pharmacological Society

KEYWORDS

nociception, Splice variants TRP channels, TRPM3

1 | INTRODUCTION

Transient receptor potential melastatin 3 (TRPM3) as designated by the International Union of Pharmacology (IUPHAR) (Alexander et al., 2019) is a non-selective cation channel and member of the **transient receptor potential (TRP) superfamily**. It forms a temperature-sensitive channel expressed in sensory neurons and has been implicated in detecting noxious heat and in the secretion of the peptide vasodilator calcitonin gene-related peptide (CGRP; Held et al., 2015; Vriens et al., 2011; Vriens et al., 2014). Therefore, TRPM3 recently shifted in the focus of attention as a promising target for the treatment of pain.

Similar to other TRP channels like **TRPV1**, **TRPA1** and **TRPM8**, the *Trpm3* gene encodes multiple isoforms (Lu, Henderson, Liu, Reinhart, & Simon, 2005; Oberwinkler, Lis, Giehl, Flockerzi, & Philipp, 2005; Sabnis, Shadid, Yost, & Reilly, 2008; Zhou, Suzuki, Uchida, & Tominaga, 2013). It contains 28 exons and three transcription start sites located upstream of exons 1, 2 and 3. Exons 1 and 2 are never identified within the same transcript (Oberwinkler & Philipp, 2014). This exon-specific start leads to different variants called TRPM3 α (α 1– α 6) starting with exon 1 and lacking exon 2 and isoforms called TRPM3 β (β 1– β 17) starting with exon 2, as well as isoforms starting at the end of exon 4 (Oberwinkler et al., 2005; Oberwinkler & Philipp, 2014). The majority of different TRPM3 isoforms originate from alternative splicing at internal splice sites, generating a high number of different TRPM3 proteins (Oberwinkler & Philipp, 2014). Splicing of *Trpm3* transcripts appears to be evolutionary well conserved between mouse and human and occurs at several different positions located in exons 8, 13, 15, 17, 20, 24 and 28. Most of the splice events do not cause a switch in the reading frame but result in the presence or absence of short stretches of 10–27 amino acid residues (Figure 1a) (Frühwald et al., 2012; Oberwinkler et al., 2005; Oberwinkler & Philipp, 2014). Interestingly, splicing within exon 28 results in a truncated version of the TRPM3 protein, while the channel functionality is fully preserved (Grimm, Kraft, Sauerbruch, Schultz, & Harteneck, 2003). Furthermore, alternative splicing of *Trpm3* within exon 24 results in short (TRPM3 α 2– α 6 and β 2– β 14) and long pore loop variants (TRPM3 α 1 and β 1) (Figure 1a).

At present, it is not clear whether these TRPM3 variants occur consistently within tissues. Although it has been reported that different splice variants might play a role in fine-tuning channel function by building heterotetramers with other isoform subunits (Frühwald et al., 2012), the actual existence of heterotetrameric TRPM3 channels *in vivo* still has to be established. Nevertheless, considering that isoforms are presenting multiple variants of the same protein and only differ in restricted areas of the amino acid sequence, they present ideal tools to study structure–function relationships to elucidate the

What is already known

- TRPM3 is a calcium permeable ion channel expressed in neuronal cells of the central and peripheral nervous system.

What this study adds

- Alternative splicing of mouse *Trpm3* gene product leads to pore loop variants, of which the occurrence is tissue-dependent.

What is the clinical significance

- Alternative splicing in the pore forming region of TRPM3 defines the pharmacological properties of the TRPM3 splice variants.

molecular mechanisms underlying channel gating and ligand interaction.

Here, we compare long and short pore-forming loop TRPM3 variants TRPM3 α 1 and TRPM3 α 2, respectively. These two variants differ only in 13 amino acids within the pore loop of the channel, including a 12 amino acid insertion and one amino acid changed from a proline to an alanine following that insertion (Oberwinkler et al., 2005) (Figure 1a). Despite this high sequence similarity, TRPM3 α 1 and TRPM3 α 2 exhibit distinct pore properties as reported in an earlier study (Oberwinkler et al., 2005). Whereas the short pore variant TRPM3 α 2 has been extensively characterized using chemical ligands such as **pregnenolone sulphate** (PS) and **CIM0216** as activators, there is no clear activation mechanism described for the long pore variant TRPM3 α 1. Here, we aim to obtain a detailed pharmacological profile and mechanistic insights for long and short pore TRPM3 α variants in order to better comprehend channel–ligand interactions.

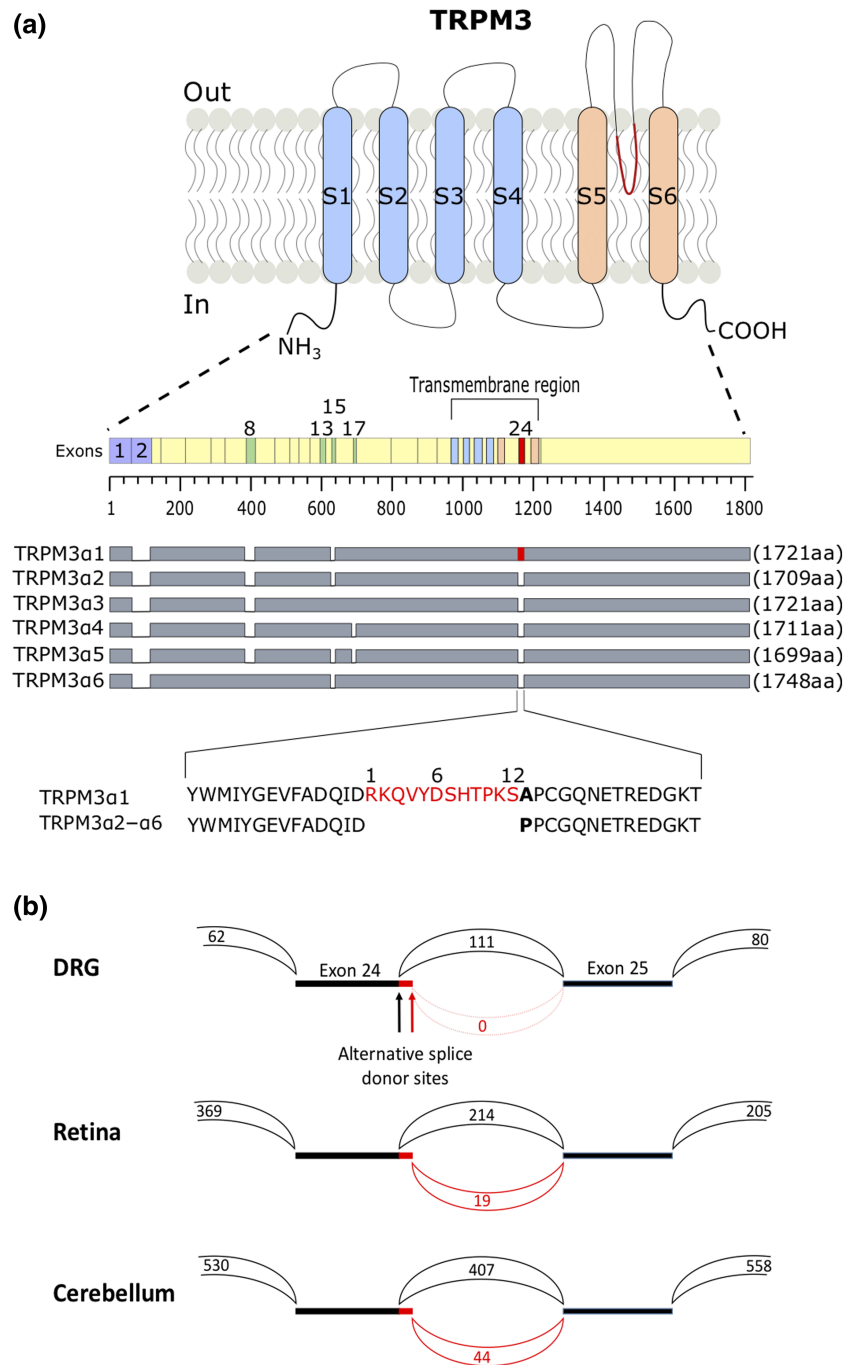
2 | METHODS

2.1 | Cell culture

HEK293T cells stably expressing murine TRPM3 α 2 (HEK-TRPM3) were designed and cultured as described previously (Vriens et al., 2011). HEK293T cells ([RRID:CVCL_0063](https://www.ebi.ac.uk/ols/ontologies/ncit/terms?concept_id=12900)) were transiently

FIGURE 1 Alternative splicing resulting in short pore and long pore TRPM3 variants.

(a) Cartoon illustrating the protein differences in TRPM3 α variants. Transmembrane segments S1–S4 of the voltage-sensing domain and S5–S6 of the pore domain are illustrated in light blue and light orange; alternative exons are numbered. Protein length of different TRPM3 α variants and their spliced exons are indicated as grey bars. Marked in red is the 12 amino acid stretch located in the pore loop on exon 24 that is unique to the TRPM3 α variant TRPM3 α 1. A segment of the pore loops of TRPM3 α 1– α 6 is represented as amino acid sequence. Numbers above the sequences are referring to the 12 amino acid insertion within exon 24. (b) Sashimi plot showing the junctions between exons 23 and 25. The two alternative splice donor sites at the 3' end of exon 24, which give rise to the short and the long pore variants, are indicated. The numbers indicate the total number of reads split across splice junctions



transfected with 2 μ g of DNA using TransIT transfection reagent (Mirusbio) or Lipofectamin (Invitrogen) 48 h before the measurements. For co-transfection experiments, DNA amounts were adapted as stated in the manuscript and figure legends. With the exception of the calcium fluorimetric experiments in Figures 2, 5 and S11, all measurements for TRPM3 α 2 were performed in HEK-TRPM3 stable cell line (Vriens et al., 2011).

2.2 | Site-directed mutagenesis

All mutants were obtained by the standard PCR overlap extension method using mTRPM3 α 2 from pCAGGS/IRES-GFP vector (Vriens,

Owsianik, Janssens, Voets, & Nilius, 2007). Accuracy of all mutant sequences was verified by sequencing of all DNA constructs.

2.3 | Immunoprecipitation experiments

Immunoprecipitation experiments have been performed as described (Frühwald et al., 2012) using monoclonal anti-Myc (Roche Applied Science, [RRID: AB_390912](#)) or anti-HA (Roche Applied Science, [RRID: AB_514505](#)). The immuno-related procedures used comply with the recommendations made by the *British Journal of Pharmacology* (Alexander et al., 2018).

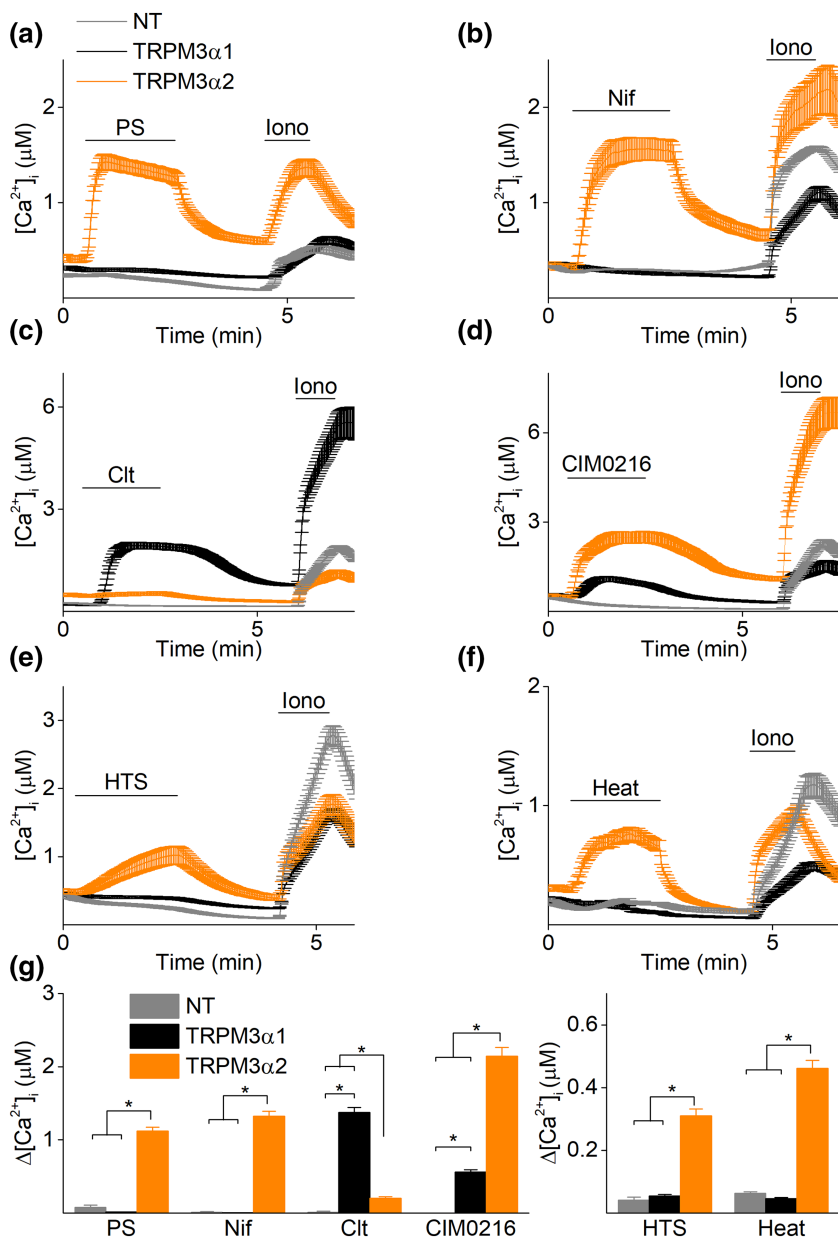


FIGURE 2 Long and short pore loop TRPM3 α isoforms possess a distinct pharmacological profile. Time course of calcium amplitudes monitored in HEK293T cells transiently transfected with either TRPM3 α 1 (black) or TRPM3 α 2 (orange) in the presence of (a) pregnenolone sulphate (PS; 40 μ M), (b) nifedipine (Nif; 50 μ M), (c) clotrimazole (Clt; 10 μ M), (d) CIM0216 (1 μ M), (e) hypotonic solution (HTS) or (f) heat (45°C). In all experiments, ionomycin (Iono; 2 μ M) was used at the end of the experiment as a control for cell viability. (g) Statistics of calcium increases induced by different stimuli (x axis) in non-transfected cells (NT) and cells transfected with TRPM3 α 1 or TRPM3 α 2; for PS: $n = 300$ for NT, $n = 323$ for TRPM3 α 1 and $n = 171$ for TRPM3 α 2; for Nif: $n = 300$ for NT, $n = 370$ for TRPM3 α 1 and $n = 177$ for TRPM3 α 2; for Clt: $n = 300$ for NT, $n = 268$ for TRPM3 α 1 and $n = 231$ for TRPM3 α 2; for CIM0216: $n = 300$ for NT, $n = 266$ for TRPM3 α 1 and $n = 204$ for TRPM3 α 2; for HTS: $n = 300$ for NT, $n = 563$ for TRPM3 α and $n = 358$ for TRPM3 α 2; for heat: $n = 455$ for NT, $n = 711$ for TRPM3 α 1 and $n = 768$ for TRPM3 α 2; in $N = 3$ independent recordings for each experiment, * $P < 0.05$ Kruskal–Wallis ANOVA with Dunn’s post hoc test

2.4 | Calcium microfluorimetry

The imaging system for standard calcium measurements has been described before (De Clercq et al., 2017). Briefly, cells were incubated with 2 μ M Fura-2-acetoxymethyl ester (Thermo Fisher Scientific) for 20 min at 37°C. Fluorescent signals were evoked during alternating illumination at 340 and 380 nm using a Lambda XL illuminator (Sutter Instrument, Novato, CA, USA) and recorded using an Orca Flash 4.0 camera (Hamamatsu Photonics Belgium, Mont-Saint-Guibert, Belgium) on a Nikon Eclipse Ti fluorescence microscope (Nikon Benelux, Brussels, Belgium). The imaging data were recorded and analysed using NIS-elements software (NIS-Elements) (RRID:SCR_014329). Absolute calcium concentrations were calculated from the ratio of the fluorescence signals at both

wavelengths (F340/F380) after correction for the individual background fluorescence signals, using the Grynkiewicz equation (Grynkiewicz, Poenie, & Tsien, 1985):

$$[Ca^{2+}] = K_{eff} \frac{R - R_0}{R_1 - R_0}$$

where the calibration constants R_0 , R_1 and K_{eff} were determined as followed: R_0 defines the ratio in Ca^{2+} free medium supplemented with 10 mM EGTA, whereas R_1 comprises the ratio in high Ca^{2+} medium (10 mM). K_{eff} , the effective binding constant, includes R_0 , R_1 , the dissociation constant of the indicator dye K_D and the isocoefficient α , according to the following equation:

$$K_{eff} = K_D \frac{R_1 + \alpha}{R_0 + \alpha}$$

The K_D of Fura-2 and the isocoefficient α were determined as described earlier (Zhou & Neher, 1993).

The standard imaging solution contained (in mM) 150 NaCl, 10 HEPES, 2 CaCl₂ and 1 MgCl₂ (pH 7.4 with NaOH). For measuring the swelling-activated calcium influx, an isotonic solution was used containing (in mM): 100 NaCl, 10 HEPES, 2 CaCl₂, 1 MgCl₂ and 100 D-mannitol, pH 7.4 with NaOH (~320 milliosmolar). Cell swelling was induced by omitting mannitol from this solution (~220 milliosmolar). Heat stimuli were applied using a Peltier heater (Warner Instruments).

Calcium ratios were calculated as the difference between the maximum value and basal value of responding cells during the stimulus period. Only cells that responded to the positive control, ionomycin, at the end of the experiment were taken into account. All experiments were performed on at least three independent coverslips.

2.5 | Patch clamp recordings

Standard patch clamp recordings were measured with an EPC 10 amplifier (EPC 10 USB Patch Clamp Amplifier, [RRID:SCR_018399](#)) and the PatchMaster Pro Software (HEKA Elektronik, Lambrecht, Germany) or with a MultiClamp 700B amplifier and the Clampex 10.6 Software (pCLAMP, [RRID:SCR_011323](#)). Current measurements were performed at a sampling rate of 10–20 kHz and currents were digitally filtered at 2.9 kHz.

For whole-cell recordings on HEK293T cells, the standard internal solution contained (in mM): 100 CsAsp, 45 CsCl, 10 EGTA, 10 HEPES and 1 MgCl₂ (pH 7.2 with CsOH) or 140 potassium gluconate, 5 EGTA, 1 MgCl₂, 10 HEPES and 2 NaATP (pH 7.3 with CsOH) for the measurements of G_{βγ}-mediated inhibition. The standard extracellular solution contained (in mM): 150 NaCl, 1 MgCl₂ and 10 HEPES (pH 7.4 with NaOH). The standard patch pipette resistance was between 2 and 4 MΩ when filled with pipette solution. To determine the calcium permeability, all Na⁺ ions in the standard extracellular solution were replaced by 100 mM Ca²⁺ and the relative permeability ($P_{Ca^{2+}}/P_{Na^+}$) was calculated from the shift in E_{rev} of the whole-cell current ($\Delta E_{rev} = E_{rev, Ca^{2+}} - E_{rev, Na^+}$) using the following equation:

$$\frac{P_{Ca^{2+}}}{P_{Na^+}} = \frac{e^{\left(\frac{\Delta E_{rev} + F}{RT}\right)} * [Na^+]_o * \left[1 + e^{\left(\frac{E_{rev, Ca^{2+}} + F}{RT}\right)}\right]}{4 * [Ca^{2+}]_o}$$

Concentration–response curves were fitted with a function of the following form:

$$y = A1 + \frac{A2 - A1}{1 + \left(\frac{V_{50}}{x}\right)^h}$$

where A1 is the bottom asymptote, A2 the top asymptote, V_{50} the half maximal effective concentration (EC_{50}) or the half maximal inhibitory concentration (IC_{50}) and h the hill slope.

2.6 | Compliance with design and statistical analysis requirements

The data and statistical analysis comply with the recommendations of the *British Journal of Pharmacology* on experimental design and analysis in pharmacology (Curtis et al., 2015; Curtis et al., 2018). The minimal sample sizes were defined as $n = 3$ individual HEK293T cells per group by performing a two-sample Student's t -test (for two group comparisons) and a one-way ANOVA power analysis (for three to four group comparisons). Parameters were taken as follows:- statistical significance was tested for a 20% difference between groups with a standard deviation of 5%, an α of 0.05 and a power of 0.9. All main conclusions of the manuscript are supported by experimental recordings of minimally $n = 5$ individual cells per group, with exact group sizes stated in the according figure legends. Some supporting data found in the Supporting Information section of this manuscript are based on group sizes smaller than $n = 5$. However, these data were not subjected to analysis for statistical comparison. Group sizes may show some variations due to the complexity of the patch clamp technique that caused differences in the success rate of the protocols. For calcium microfluorimetry, a total of three independent coverslips were recorded for each experiment. Each recording allowed to test more than 50 individual cells per coverslip.

Data recordings were randomized by random selection of HEK293T cells on each individual coverslip, but operators were not blinded during data collection or analysis because long and short pore loop TRPM3 isoforms possess a distinct current rectification that is unmistakable. Furthermore, the experimental outcomes of here performed electrophysiological cell recordings are operator independent and not influenced by subjective interpretations. Data analysis of calcium microfluorimetry data was automatically performed with a prewritten analysis script (Igor Pro, [RRID:SCR_000325](#)), thereby further cancelling out any operator bias.

Electrophysiological and calcium microfluorimetric data were analysed using NIS-Elements software (NIS-Elements, [RRID:SCR_014329](#)), Excel (Microsoft), Igor Pro 6.2 (WaveMetrics, USA), Clampfit 10.6 (Molecular Devices, USA), WinASCD (Guy Droogmans, Leuven, Belgium) and OriginPro 8.6 (Origin, [RRID:SCR_014212](#)). OriginPro 8.6, R Core Team (2018) (R Foundation for Statistical Computing, Vienna, Austria. URL <https://www.R-project.org/>) and RStudio Team (2016) (RStudio, [RRID:SCR_000432](#)) were further used for statistical analysis and data display. All data sets were tested for normality and a Student's two-tailed unpaired t -test or a Mann-Whitney U -test was used for statistical comparison between two different data sets. For comparison of multiple groups (groups > 2), a one-way ANOVA or a non-parametric Kruskal-Wallis test was applied. If F in ANOVA achieved $P < 0.05$ and there was no significant variance inhomogeneity, a Tukey's post hoc test was performed. In case of $P < 0.05$ in Kruskal-Wallis test a Dunn's post hoc test was performed. For normal distributed data, the variance homogeneity was tested with a Barlett's test. P values below 0.05 were considered as significantly different. Data points represent means \pm SEM of the given

number (n) of individual experiments. No outlier exclusion was performed in any of the experiments.

Data normalization was performed in order to plot conductance–voltage curves (normalized conductances) for the ion channel variants. This was accomplished by normalizing the data to the highest conductance value for each individual recorded cell. As recordings were performed in steady-state conditions (at very high voltages), the highest value was not always obtained at the same voltage, thereby still yielding data variances for all collected data points.

2.7 | Splice analysis

Publicly available RNA-sequence data from mouse dorsal root ganglions (DRGs), retina, hippocampus, choroid plexus and cerebellum (see Table 1 for accession numbers) were aligned against the mouse genome sequence GRCm38.p6 using STAR (STAR, [RRID:SCR_015899](https://doi.org/10.15899)) (Dobin et al., 2013) version 2.7. The reference genome and the resulting alignments were loaded into the Integrative Genomics Viewer (Robinson et al., 2011) version 2.6 and alternative splicing events at the junction between exons 24 and 25 were visualized and counted using the Viewer's Sashimi plot feature.

2.8 | Materials

Clotrimazole, [D-Ala², N-Me-Phe⁴, Gly⁵-o]-Enkephalin acetate salt (DAMGO), Diclofenac, Naloxone, Nifedipine, N-methyl-D-glucamine,

Pregnenolone sulphate sodium salt and Primidone were purchased from Sigma Aldrich. CIM0216 was purchased from Tocris Bioscience. Isosakuranetin was purchased from Carl Roth and Ionomycin was purchased from Fisher Scientific. N-methyl-D-glucamine was directly diluted in external recording solutions. Stock solutions were prepared from all other drugs by diluting them in DMSO according to distributor instructions.

2.9 Nomenclature of targets and ligands

Key protein targets and ligands in this article are hyperlinked to corresponding entries in the IUPHAR/BPS Guide to PHARMACOLOGY <http://www.guidetopharmacology.org> and are permanently archived in the Concise Guide to PHARMACOLOGY 2019/20 (Alexander et al., 2019).

3 | RESULTS

3.1 | Expression pattern of the short and long pore variants of TRPM3 in mouse

Alternative splicing within exon 24 of the mouse *Trpm3* gene leads either to a short pore loop or to a longer pore loop characterized by the insertion of a stretch of 12 amino acids and the replacement of an alanine by a proline residue (Figure 1a) (Oberwinkler et al., 2005). To evaluate the occurrence of short and long pore variants of TRPM3 in different tissues, we analysed publicly available RNA-sequence data

TABLE 1 Tissue expression and alternative splicing of TRPM3 in different tissues

Tissue		Expression level (relative to GAPDH)	Exon 24–25 reads	% Long pore	95% CI	Database no.
DRG (Vandewauw et al., 2018)		0.024	111	0.00	[0.00, 3.27]	PRJNA431738
Retina (Wang, Geisert, & Struebing, 2019)		0.032	233	8.15	[4.98, 12.4]	GSE127942
Hippocampus (Cembrowski, Wang, Sugino, Shields, & Spruston, 2016)	CA2	0.074	112	0.89	[0.02, 4.87]	GSE74985
	CA3	0.014	61	3.28	[0.40, 11.4]	
	DGg	0.136	100	1.00	[0.02, 5.45]	
	DGm	0.002	12	41.7	[15.2, 72.3]	
Choroid plexus (Lun et al., 2015)	hChP	1.30	450	0.44	[0.05, 1.60]	GSE66312
	hCPEC	2.17	453	0.44	[0.05, 1.59]	
	tChP	2.18	406	0.25	[0.01, 1.37]	
	tCPEC	2.17	294	0.00	[0.00, 1.25]	
Cerebellum (The ENCODE Project Consortium, 2012)		0.012	451	9.76	[7.18, 12.9]	GSE90200

Note: Expression levels are calculated as the total number of TRPM3 reads divided by the total number of reads for GAPDH. Exon 24–25 reads gives the number of reads that span the boundary between exons 24 and 25 and the % of these reads that give rise to the long pore is given, along with the 95% confidence interval based on a Poisson distribution.

Abbreviations: CA2 and CA3, *Cornu Ammonis* area 2/3, dorsal and ventral pyramidal cells from respective areas; DGg, dorsal and ventral granule cells from the dentate gyrus; DGm, dorsal mossy cells from the dentate gyrus; hChP/tChP: hindbrain/telencephalic choroid plexus; hCPEC/tCPEC, FACS-purified hindbrain/telencephalic choroid plexus epithelial cells.

from different mouse tissues for TRPM3 expression and used the Sashimi plot feature of the Integrative Genomics Viewer (reference: PMID 21221095) to visualize and quantify alternative splicing at the junction between exons 24 and 25 (Figure 1b; Table 1). This analysis revealed that at least in the investigated tissues, the splice event leading to the shorter pore loop is the most frequent but interestingly also that the occurrence of the longer pore splice variants is tissue dependent. For instance, in sensory neurons from the DRG, only reads corresponding to the short pore loop were found, compared to approximately 10% reads related to the longer pore loop in retina and cerebellum (Figure 1b; Table 1).

3.2 | Agonist sensitivity is conserved in the short pore loop TRPM3 α variants

To investigate differences in ligand activation between several TRPM3 α variants ($\alpha 1$ – $\alpha 6$), calcium microfluorimetric experiments of transiently transfected HEK293T cells were performed. Application of the established TRPM3 agonists, pregnenolone sulphate and **nifedipine** (Nif), did not induce any detectable calcium rise in cells expressing the long pore loop TRPM3 $\alpha 1$ variant (Figures 2a, b and g and S1) (Oberwinkler et al., 2005). Even stimulation at high concentrations of both agonists did not induce any detectable calcium signal (Figure S2). However, applying these stimuli to the short pore loop TRPM3 α variants resulted in robust calcium responses in all different isoforms ($\alpha 2$ – $\alpha 6$) (Figures 2a, b and g and S1). For TRPM3 $\alpha 2$, these results are fully in line with previous studies (Held et al., 2018; Oberwinkler et al., 2005; Vriens et al., 2011; Vriens et al., 2014). All of the short pore loop TRPM3 α variants showed similar functionality (Figure S1) and therefore, TRPM3 $\alpha 2$ served as representative isoform of short pore loop TRPM3 α channels in most of the subsequent experiments.

Next, the effects of other TRPM3 activating stimuli, including the synthetic agonist CIM0216 (Held et al., 2015; Rubil & Thiel, 2017) and the physical stimuli hypotonicity (Grimm et al., 2003) and heat (Vriens et al., 2011) were assessed on the pore loop variants. Notably, sizable increases in intracellular calcium were observed for TRPM3 $\alpha 1$ when stimulated with CIM0216. However, the amplitudes of these responses were significantly lower than for TRPM3 $\alpha 2$. Interestingly, while TRPM3 $\alpha 2$ -expressing cells showed robust responses to heat and to stimulation by a hypotonic solution (HTS), such responses were absent in TRPM3 $\alpha 1$ expressing cells (Figure 2d–g).

Conversely, **clotrimazole** (Clt), an antifungal drug previously reported as a modulator of the short pore loop TRPM3 α variants (Held et al., 2018; Krugel, Straub, Beckmann, & Schaefer, 2017; Vriens et al., 2014), induced robust calcium increases in cells transfected with TRPM3 $\alpha 1$. These clotrimazole-induced calcium responses were significantly larger compared to non-transfected cells and TRPM3 $\alpha 2$ -expressing cells (Figure 2c,g). These results suggest that the long pore loop TRPM3 $\alpha 1$ variant is a calcium permeable ion channel that can be activated by clotrimazole and CIM0216. However, in contrast to the short pore loop TRPM3 α variants, TRPM3 $\alpha 1$ cannot

be activated by some of the reported activation stimuli of TRPM3 $\alpha 2$, including pregnenolone sulphate, nifedipine, hypotonicity or heat.

3.3 | Clotrimazole and CIM0216 identified as chemical agonists of the long pore loop TRPM3 $\alpha 1$

Subsequently, the pharmacological differences between TRPM3 α isoforms were further investigated using patch clamp recordings. In line with the calcium experiments, stimulation by pregnenolone sulphate did not evoke any increase in current amplitude in HEK293T cells expressing TRPM3 $\alpha 1$ (Figure 3a,e), whereas robust current increases were detected in exploratory experiments of all the short pore loop TRPM3 α isoforms ($\alpha 2$ – $\alpha 6$) (Figures 3c–e and S3) (Held et al., 2015; Vriens et al., 2014; Wagner et al., 2008). Analysis of the current–voltage (I – V) relationship of the short variants showed outwardly rectifying currents in the presence of pregnenolone sulphate, although with variable rectification ratios (Figure S4). Similarly, nifedipine was without effect on whole-cell currents in cells expressing TRPM3 $\alpha 1$ (Figure 3a,e). Remarkably, direct application of clotrimazole induced a strong and reversible increase in the current amplitude in a concentration-dependent manner ($EC_{50} = 3 \mu M$ at ± 80 mV) in TRPM3 $\alpha 1$ expressing cells (Figure 3f). The clotrimazole-induced currents exhibited a linear I – V relationship (Figures 3b and S4). When replacing all monovalent cations in the external solution by NMDG⁺, the clotrimazole-induced inward currents were strongly reduced (Figure S5). Moreover, co-application of pregnenolone sulphate resulted in a minor inhibition of the clotrimazole-activated currents ($10.5 \pm 5.1\%$ at $+80$ mV) in TRPM3 $\alpha 1$ expressing cells (Figures 3a, b and e and S7). Further, in inside-out patch clamp recordings from TRPM3 $\alpha 1$ expressing cells, clotrimazole reversibly activated robust currents with a linear I – V relationship (Figure S5), indicating that clotrimazole can activate TRPM3 $\alpha 1$ in a membrane-delimited manner. In contrast, stimulation by clotrimazole did not induce any current increase in the short TRPM3 α variants (Figures 3c,e and S3). However, clotrimazole strongly potentiated pregnenolone sulphate-induced currents in all of these TRPM3 α variants, resulting in currents with a typical double rectification (Figures 3d, S3 and S4). In earlier work, we have demonstrated that co-application of pregnenolone sulphate + clotrimazole induced a strong inwardly rectifying current component representing ion flux through an alternative ion permeation pathway located in the voltage sensor domain of TRPM3 $\alpha 2$ (Vriens et al., 2014). This non-canonical pore can be distinguished from the central pore based on its voltage dependence, ion selectivity, insensitivity to pore block by La³⁺ and the lack of calcium-dependent desensitization. We therefore hypothesized that activation by clotrimazole induced the opening of an alternative ion permeation pathway in TRPM3 $\alpha 1$. Our results illustrated that the clotrimazole-activated currents in TRPM3 $\alpha 1$ showed an almost linear voltage dependence, resulting in high conductances over the whole voltage range (Figure S6). The inward currents were reduced when extracellular Na⁺ was replaced by monomethylammonium. Furthermore, the inward and outward current components were highly resistant to block by

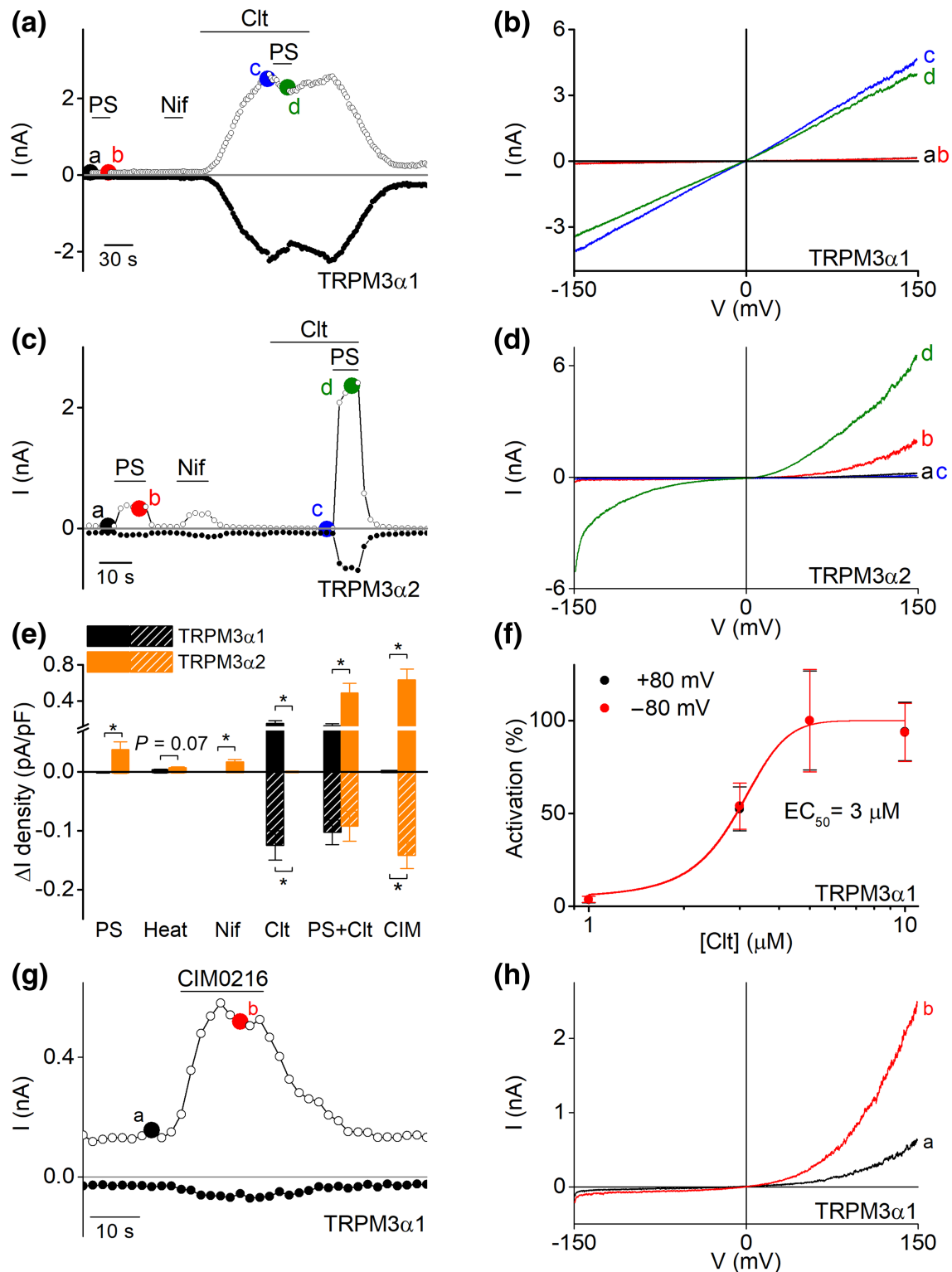


FIGURE 3 Identification of clotrimazole and CIM0216 as chemical agonist of TRPM3 α 1. (a) Time course of whole-cell patch clamp recording at holding potentials of +80 mV (open circles) and -80 mV (closed circles) of TRPM3 α 1 expressed in HEK293T cells during application of different TRPM3 modulators, pregnenolone sulphate (PS; 40 μ M), nifedipine (Nif; 50 μ M) and Clt (10 μ M). (b) Current-voltage relationship (I - V) of time points indicated in panel (a). (c) Similar as in panel (a) but on TRPM3 α 2. (d) I - V of time points indicated in panel (c). (e) Statistics of current increases at \pm 80 mV induced by different stimuli (x axis) in TRPM3 α 1 and TRPM3 α 2 (n = 5 for each treatment on TRPM3 α 1; n = 11 for each treatment on TRPM3 α 2, * P < 0.05 with Student's two-tailed unpaired t -test). (f) Concentration-response curve for Clt on TRPM3 α 1 in HEK293T cells (n = 6 for 1 and 3 μ M; n = 11 for 5 μ M and n = 10 for 10- μ M treatment). (g) Time course of whole-cell patch clamp recording in HEK293T cells transiently transfected with TRPM3 α 1 upon application of CIM0216 (1 μ M). (h) I - V of time points indicated in panel (g).

the central pore blocker La^{3+} and to calcium-dependent desensitization (Figure S6).

Next, application of CIM0216 to TRPM3 α 1 expressing cells induced activation of small, outwardly rectifying currents in a concentration-dependent manner ($\text{EC}_{50} = 0.57 \pm 0.05 \mu\text{M}$) (Figures 3g,h and S7). However, at higher doses of CIM0216 ($\geq 5 \mu\text{M}$), activation of TRPM3 α 1 was followed by a rapid current decay (Figure S7). Note that clotrimazole did not show any competitive or synergistic actions with CIM0216 on the TRPM3 α 1 variant. Contrarily, stimulation of CIM0216 to TRPM3 α 2 induced a robust increase in both inward and outward currents (Figure S7) (Held et al., 2015).

Next, we investigated the relative calcium permeability of the CIM0216-induced current in both pore variants. The TRPM3 α 1 variant was calculated as $P_{\text{Ca}^{2+}}/P_{\text{Na}^{+}} = 0.7$, which was significantly reduced compared to TRPM3 α 2 ($P_{\text{Ca}^{2+}}/P_{\text{Na}^{+}} = 3.9$) (Figure S8). Altogether, these data indicate that TRPM3 α 1 is a calcium permeable ion channel that has a distinct activation pattern compared to the short TRPM3 α variants in which clotrimazole and CIM0216 were identified as new activators of the long pore loop splice variant.

3.4 | Long and short pore loop TRPM3 variants differ in their sensitivity to TRPM3 antagonists

Next, we tested the affinity for reported TRPM3 inhibitors for both pore loop variants by patch clamp recordings. Application of **isosakuranetin** ($5 \mu\text{M}$) fully inhibited CIM0216-induced currents in TRPM3 α 2-expressing cells. Interestingly, also the CIM0216-induced currents of TRPM3 α 1 expressing cells were fully blocked by isosakuranetin. In contrast, a similar concentration of isosakuranetin induced only a partial inhibition (25%) of the clotrimazole-induced currents in cells expressing TRPM3 α 1 (Figure 4a–c). Additional exploratory experiments showed an IC_{50} value for isosakuranetin of $32.5 \pm 8.5 \mu\text{M}$ for clotrimazole-induced TRPM3 α 1 currents (Figure S9), which was significantly higher compared to earlier reported values for TRPM3 α 2 (Straub et al., 2013). Analogous results were acquired for two other TRPM3 inhibitors, **diclofenac** ($100 \mu\text{M}$) and **primidone** ($25 \mu\text{M}$) (Krugel et al., 2017; Suzuki et al., 2016). Both TRPM3 inhibitors caused a full block of CIM0216-evoked TRPM3 α 1 and TRPM3 α 2 currents, while in contrast, the clotrimazole-induced TRPM3 α 1 currents were only partially blocked (Figure 4d–i). TRPM3 α 2 activity is inhibited upon activation of GPCRs, via a mechanism that involves direct binding of the $\text{G}_{\beta\gamma}$ of trimeric G proteins to the channel (Badheka et al., 2017; Dembla et al., 2017; Quallo, Alkhatib, Gentry, Andersson, & Bevan, 2017). To evaluate whether $\text{G}_{\beta\gamma}$ -dependent modulation is altered in TRPM3 α 1, HEK293T cells were co-transfected with the **μ opioid receptor** and the long pore variant and evaluated for the effect of the selective μ opioid agonist **DAMGO** on CIM0216 and clotrimazole-activated whole-cell currents. In cells expressing TRPM3 α 1, application of DAMGO induced a complete and rapidly reversible inhibition of the CIM0216-induced

currents, whereas the clotrimazole-induced currents were only partially inhibited (Figures 4j–l and S10). In conclusion, these data demonstrate that TRPM3 antagonists can act on both long and short pore loop variants. However, the blocking potency of the antagonists on TRPM3 α 1 is highly dependent on the activating ligand.

3.5 | Cells co-expressing TRPM3 α 1 and TRPM3 α 2 showed reduced steroid-induced calcium entry

Next, we co-transfected HEK293 cells with cDNA encoding TRPM3 α 1 and TRPM3 α 2 and analysed in immunoprecipitation experiments whether both proteins interact physically and potentially build heteromultimeric channel complexes. To distinguish the almost identical proteins TRPM3 α 1 and TRPM3 α 2, their cDNAs were cloned into expression vectors providing HA or myc tags at the amino-terminal endings of the expressed proteins. After transfection in a 1:1 ratio into HEK293 cells, immunoprecipitations were performed with either anti-myc or anti-HA antibodies as described earlier (Frühwald et al., 2012). Similar to other TRPM3 isoforms (Frühwald et al., 2012), HA-tagged TRPM3 α 2 co-precipitated the myc-tagged TRPM3 α 1 isoform and vice versa (Figure 5a,b). To test the functional interplay of TRPM3 α 1 and TRPM3 α 2, we performed experiments in which HEK293 cells were transfected with a constant dose of TRPM3 α 2 cDNA ($0.5 \mu\text{g}$) and co-transfected with increasing doses of TRPM3 α 1 cDNA ($0, 1.5$ and $3 \mu\text{g}$). Transfected cells were tested for their responses to stimulation by pregnenolone sulphate and clotrimazole in calcium experiments. Addition of pregnenolone sulphate induced robust increases in intracellular calcium in all different conditions. However, the increase in calcium was significantly reduced in cells co-expressing TRPM3 α 2 and TRPM3 α 1. In contrast, HEK293 cells co-transfected with increasing concentrations of TRPM3 α 1 showed increasingly higher calcium influx after stimulation with clotrimazole (Figure 5c,d). These data suggest that TRPM3 α 1 channel subunits could interfere with pregnenolone sulphate-induced calcium entry and could therefore provide a control mechanism of ion permeation in TRPM3 α 1/ α 2 co-expressing tissue.

3.6 | The pore loop length is defining TRPM3 pharmacology

Next, we focused on the 13 amino acid difference in the pore loop between TRPM3 α 1 and TRPM3 α 2 to identify the structural elements underlying their distinct pharmacological properties. In particular, we analysed a set of mutant channels created either by deleting amino acids from the pore loop of TRPM3 α 1 or by inserting one or more alanines in the pore loop of TRPM3 α 2.

In a first strategy, we created sets of deletions of three residues in TRPM3 α 1, resulting in four different mutants, TRPM3 α 1 Δ 3a, b, c and d (Figure 6). All these mutants showed similar properties as the native TRPM3 α 1, as they could be activated by clotrimazole

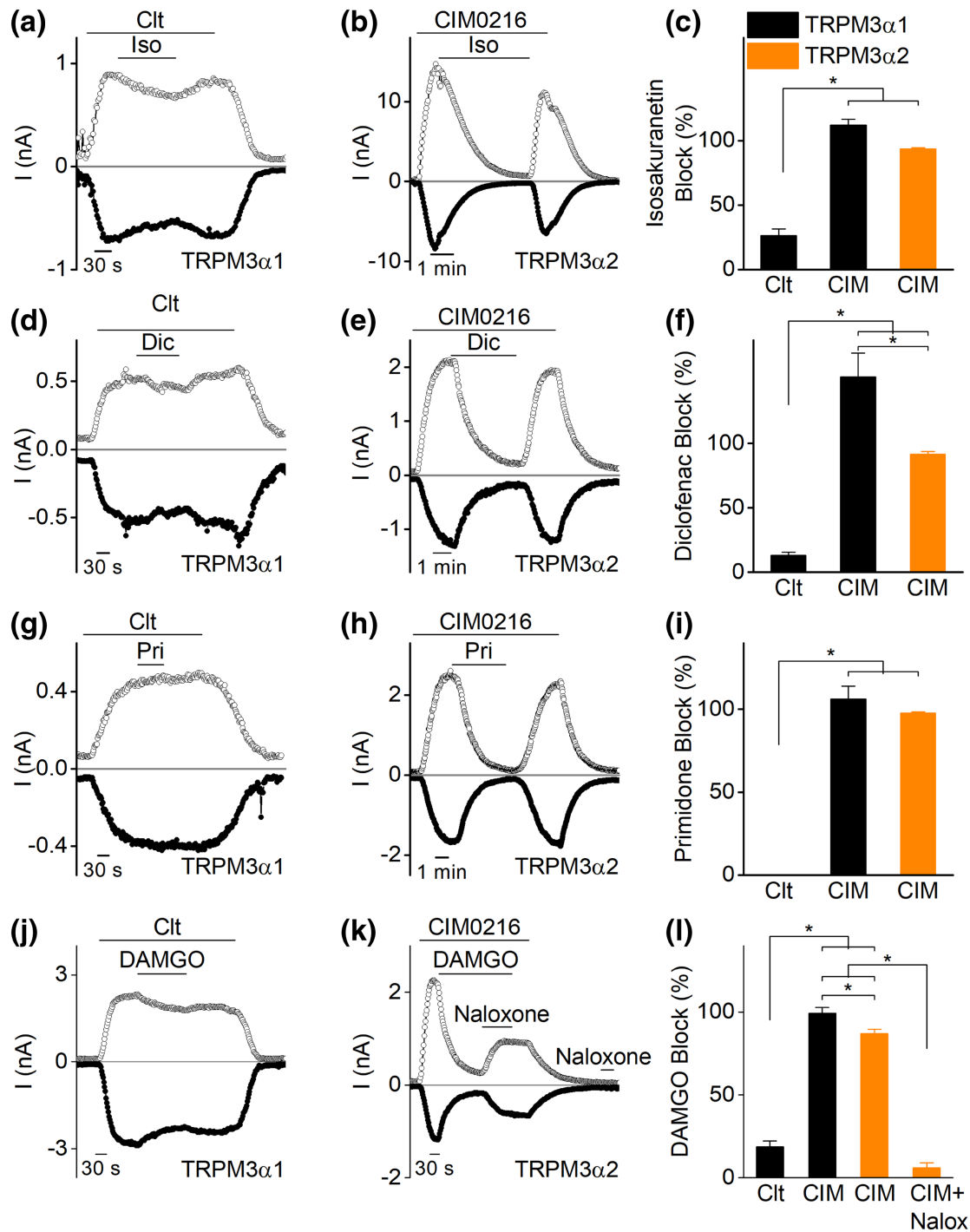


FIGURE 4 TRPM3 α 1 and TRPM3 α 2 show different sensitivity to antagonists. Time course of whole-cell currents at ± 80 mV in HEK293T cells transfected with (a) TRPM3 α 1 upon application of clotrimazole (Clt; 10 μ M) and isosakuranetin (5 μ M) or (b) TRPM3 α 2 upon application of CIM0216 (1 μ M) and isosakuranetin (5 μ M). (c) Percentage of block induced by isosakuranetin in experimental conditions of panels (a) and (b) and in experiments of CIM0216-induced TRPM3 α 1 currents ($n = 6$ for Clt on TRPM3 α 1; $n = 5$ for CIM0216 on TRPM3 α 1 and TRPM3 α 2); $*P < 0.05$ with one-way ANOVA. (d and g) Similar as in panel (a) but with diclofenac (Dic, 100 μ M, panel [d]) or primidone (Pri, 25 μ M, panel [g]) application instead. (e and h) Similar protocol as in panel (b) but for diclofenac (panel [e]) or primidone (panel [h]) application. (f and i) Percentage of block induced by diclofenac (panel [f]) and primidone (panel [i]) in experimental conditions of panels (d) and (e) and in experiments of CIM0216-induced TRPM3 α 1 currents (for panel [f]: $n = 5$ for Clt and CIM0216 on TRPM3 α 1; $n = 7$ for CIM0216 on TRPM3 α 2; for panel [i]: $n = 5$ for all conditions); $*P < 0.05$ with one-way ANOVA. (j) Time course of whole-cell currents at ± 80 mV in HEK293T cells co-expressing TRPM3 α 1 and μ opioid receptors upon application of Clt (10 μ M) and DAMGO (1 μ M). (k) Time course of whole-cell currents at ± 80 mV in HEK293T cells co-expressing TRPM3 α 2 and μ opioid receptors upon application of CIM0216 (1 μ M), DAMGO (1 μ M) and naloxone (10 μ M). (l) Percentage of block induced by DAMGO in experimental conditions of panels (j) and (k) and in experiments of CIM0216-induced TRPM3 α 1 currents ($n = 7$ for Clt on TRPM3 α 1; $n = 9$ for CIM0216 on TRPM3 α 1; $n = 8$ for both TRPM3 α 2 conditions). $*P < 0.05$ with one-way ANOVA with Tukey's post hoc test

FIGURE 5 Molecular and functional interaction of TRPM3 α 1 and TRPM3 α 2. (a and b) To distinguish the almost identical proteins TRPM3 α 1 and TRPM3 α 2, their cDNAs were cloned into expression vectors providing HA or myc tags at the very amino-terminal endings of the expressed proteins. After transfection of their cDNA in a 1:1 ratio into HEK293 cells, immunoprecipitations were performed with either (a) anti-myc or (b) anti-HA antibodies. HA-tagged TRPM3 α 2 co-precipitated the myc-tagged TRPM3 α 1 isoform and vice versa. (c) Time course of calcium microfluorimetry recordings in HEK293T cells transiently transfected with TRPM3 α 2 or transiently co-transfected with TRPM3 α 1 and TRPM3 α 2 in ratios (3:1) and (6:1) upon application of pregnenolone sulphate (PS; 40 μ M) and clotrimazole (Clt; 10 μ M). (d) Statistics of calcium increases induced by PS and Clt in conditions as in (c). $n = 393$ for TRPM3 α 2, $n = 415$ for TRPM3 α 1 : TRPM3 α 2 (3:1) and $n = 285$ for TRPM3 α 1 : TRPM3 α 2 (6:1) in $N = 3$ independent recordings for each experiment, * $P < 0.05$ with Kruskal–Wallis ANOVA with Dunn's post hoc test

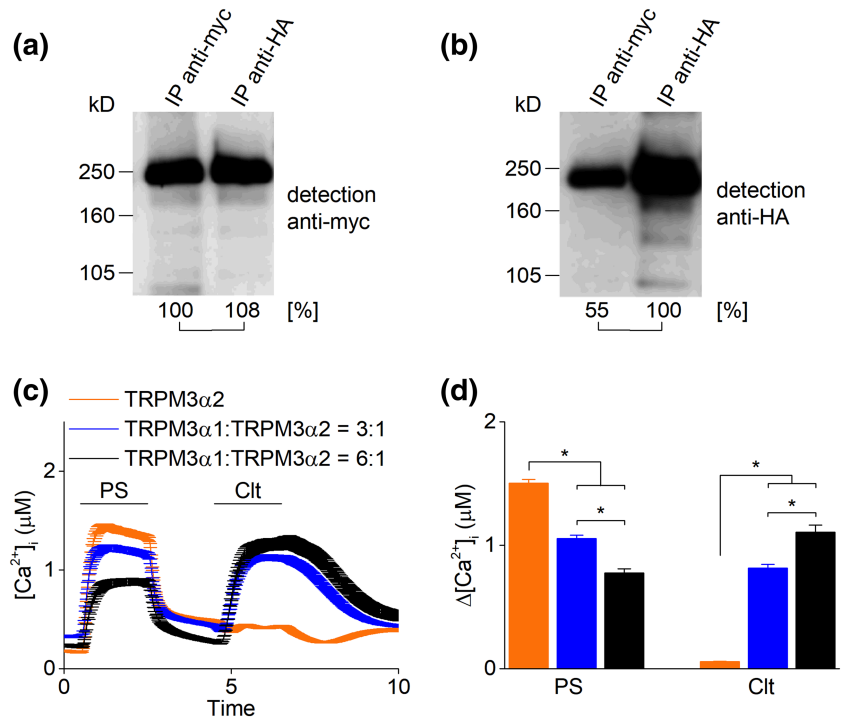
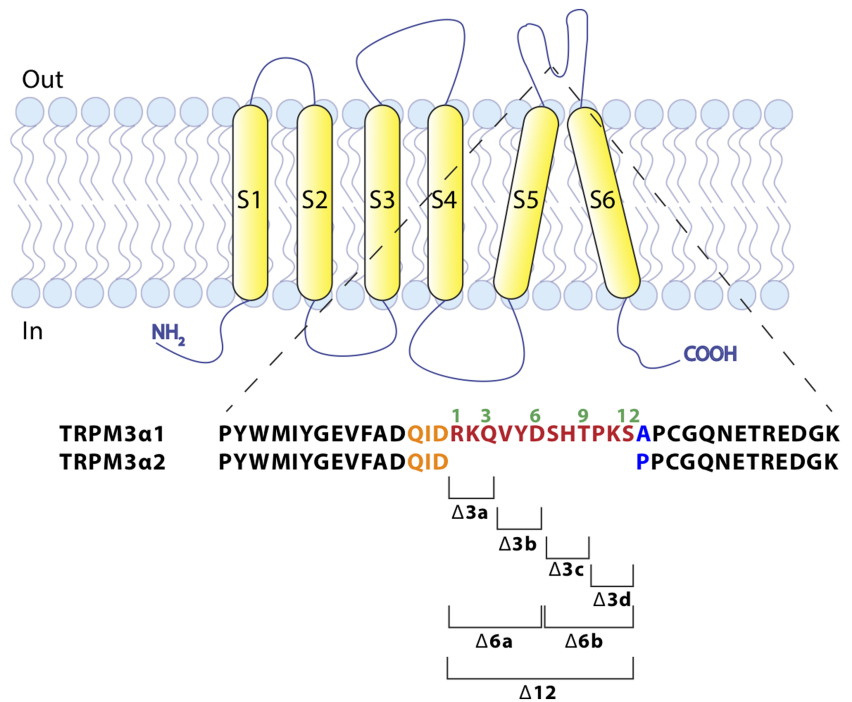


FIGURE 6 Cartoon illustrating the design of TRPM3 α 1 deletion mutants. Cartoon of a TRPM3 α subunit in the plasma membrane, illustrating the sequence difference of TRPM3 α 1 and TRPM3 α 2 in the pore loop. Brackets mark the amino acids that were removed in the indicated deletion mutants



stimulation and were irresponsive to application of pregnenolone sulphate (Figure 7a and Table 2). Subsequently, additional mutants were designed with deletions of an increasing number of amino acids in the pore loop of TRPM3 α 1, including TRPM3 α 1 Δ 6a and b (deleting residues 1–6 and 7–12) and TRPM3 α 1 Δ 12 (deleting residues 1–12). The later mutant is identical to TRPM3 α 2, with the exception of the 13th position, where alanine is present in TRPM3 α 1 instead of a

proline (Figure 6). The deletion of six amino acids in the pore loop of TRPM3 α 1 did not influence the pharmacological sensitivity to pregnenolone sulphate or clotrimazole compared to the wild-type TRPM3 α 1 (Figure 7b and Table 2). However, deleting the entire 12 additional amino acids in the pore loop of TRPM3 α 1 resulted in a channel mutant that resembled wild-type TRPM3 α 2 (Figure 7c and Table 2). These results indicate that the alanine at position 13 is

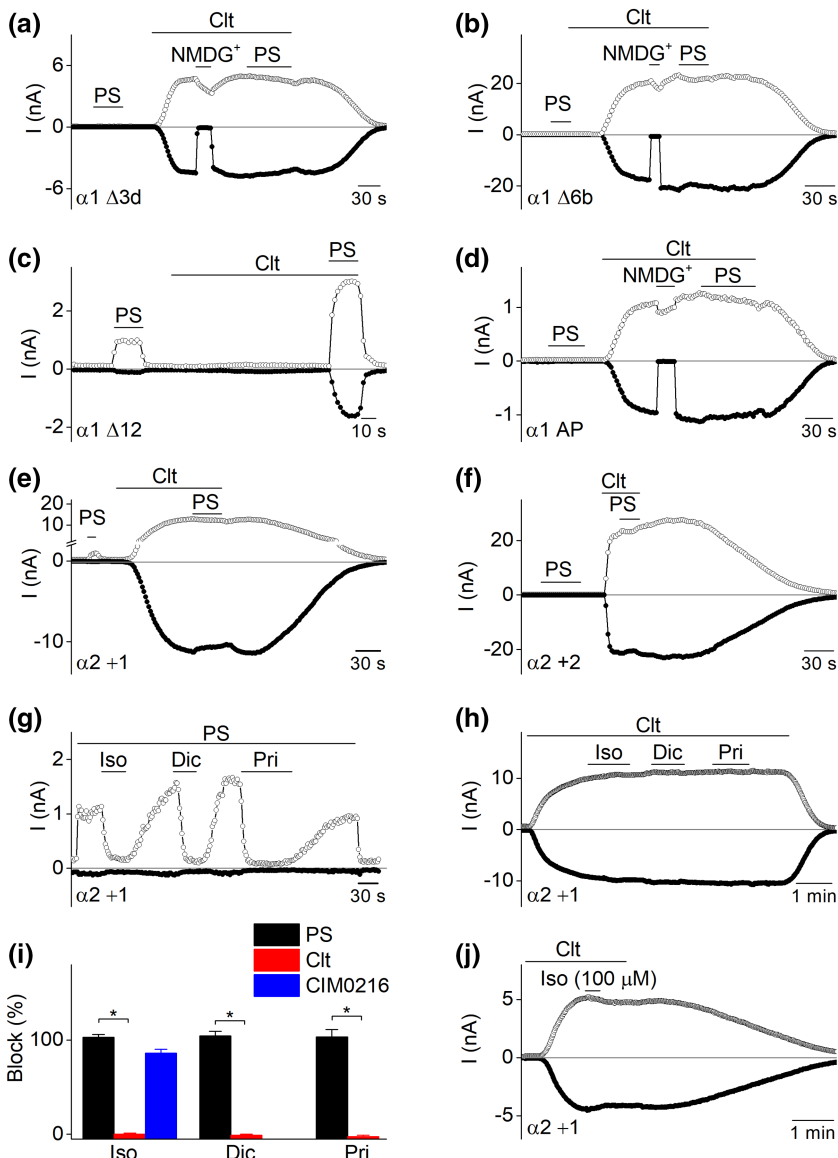


FIGURE 7 The pore loop length is a specific determinant of the TRPM3 α variant properties. (a–e) Time course of whole-cell patch clamp recording at ± 80 mV of HEK293T cells transiently expressing different TRPM3 α mutant channels upon application of pregnenolone sulphate (PS; 40 μM) and clotrimazole (Clt; 10 μM); where indicated, all extracellular Na $^+$ was replaced by NMDG $^+$. Cells are expressing mutant (a) TRPM3 $\alpha 1 \Delta 3d$, (b) TRPM3 $\alpha 1 \Delta 6b$, (c) TRPM3 $\alpha 1 \Delta 12$, (d) TRPM3 $\alpha 1 A1077P$, (e) TRPM3 $\alpha 2 D1064_A_P1065$; (g) time course of whole-cell patch clamp recording at ± 80 mV of HEK293T cells transiently expressing insertion mutant TRPM3 $\alpha 2_D1064_A_P1065$ (TRPM3 $\alpha 2 + 1$) during the assessment of the action of different TRPM3 antagonists on PS-induced TRPM3 $\alpha 2 + 1$ currents. (h) As in panel (g) for Clt-induced TRPM3 currents. (i) Statistics illustrating the percentage of block that TRPM3 antagonists such as isosakuranetin (5 μM), diclofenac (100 μM) and primidone (25 μM) induce in TRPM3 $\alpha 2 + 1$ for different TRPM3 activation stimuli ($n = 7$ for all blockers on PS- and CIM0216-induced currents and $n = 6$ for all blockers on Clt-induced currents). (j) Time course of whole-cell patch clamp recording at ± 80 mV of HEK293T cells transiently expressing TRPM3 $\alpha 2 + 1$. High concentrations of isosakuranetin (100 μM) tested on Clt-induced currents. * $P < 0.05$ with Kruskal–Wallis ANOVA with Dunn’s post hoc test or Mann–Whitney U -test for comparison between two individual groups

of lesser importance for the monitored pharmacological isoform differences. In line with this, mutating the alanine at position 13 to a proline in TRPM3 $\alpha 1$ resulted in a mutant channel that has similar pharmacological properties of the original TRPM3 $\alpha 1$ (Figure 7d and Table 2). Additionally, to explore the effect of TRPM3 antagonists on the deletion mutants, $\Delta 3d$ and $\Delta 6b$ mutants were tested for their sensitivity to reported TRPM3 antagonists. Both mutants showed only a partial block by isosakuranetin (5 μM), diclofenac (100 μM) and primidone (25 μM) when activated by clotrimazole, thereby resembling TRPM3 $\alpha 1$ (Figure S11).

In a second strategy, the short pore loop of TRPM3 $\alpha 2$ was extended by the stepwise insertion of alanine residues. In total, five channel mutants were designed and tested, ranging from TRPM3 $\alpha 2 + 1$ (one alanine is inserted between D1064 and P1065) up to TRPM3 $\alpha 2 + 5$ (with five alanines inserted). Interestingly, the TRPM3 $\alpha 2 + 1$ mutant responded with robust linear currents in response to clotrimazole and outwardly rectifying currents in

response to pregnenolone sulphate. In addition, the TRPM3 $\alpha 2 + 1$ mutant showed similar calcium influxes to wild-type TRPM3 $\alpha 2$ after stimulation by hypotonic solution and heat, thus exhibiting a mixed phenotype between TRPM3 $\alpha 1$ and TRPM3 $\alpha 2$ (Figure S11 and Table 2). All other insertion mutants (TRPM3 $\alpha 2 + 2$ to $+5$) recapitulated the properties of TRPM3 $\alpha 1$: direct activation by clotrimazole, displaying large currents with a linear I - V relationship (Table 2) and no response to pregnenolone sulphate. In line herewith, HEK293T cells transfected with the mutant TRPM3 $\alpha 2 + 3$ showed calcium response patterns to hypotonic solution and heat that were comparable to wild-type TRPM3 $\alpha 1$ (Figure S11). Interestingly, all tested TRPM3 blockers (isosakuranetin, diclofenac and primidone) were able to fully block pregnenolone sulphate-induced currents in TRPM3 $\alpha 2 + 1$ but were ineffective on clotrimazole-evoked currents (Figure 7g–i). In addition, CIM0216-evoked currents could also be fully blocked by isosakuranetin (5 μM) in TRPM3 $\alpha 2 + 1$ (Figure 7i), while even high concentrations of isosakuranetin (100 μM) were

TABLE 2 Overview of the activation pattern of TRPM3 α pore loop mutant channels;

Mutant	n	PS +80 mV Δ I density (pA/pF)	PS -80 mV Δ I density (pA/pF)	Clt +80 mV Δ I density (pA/pF)	Clt -80 mV Δ I density (pA/pF)
α 1	5	-1.0 \pm 0.85	0.2 \pm 0.1	152.9 \pm 30.6	-124.9 \pm 25.0
α 2	11	38.1 \pm 12.9	-1.9 \pm 0.5	-0.1 \pm 1.1	0.6 \pm 0.4
α 1 A-P	6	-0.4 \pm 0.6	-0.1 \pm 0.3	125.8 \pm 37.9	-117.3 \pm 36.5
α 1 Δ 3a	5	0.01 \pm 0.2	0.3 \pm 0.3	430.6 \pm 74.8	-355.3 \pm 55.5
α 1 Δ 3b	5	-0.5 \pm 0.4	0.1 \pm 0.04	149.2 \pm 21.2	-122.8 \pm 13.9
α 1 Δ 3c	5	-0.1 \pm 0.1	0.2 \pm 0.1	242.5 \pm 17.2	-225.3 \pm 13.8
α 1 Δ 3d	5	0.04 \pm 0.3	0.01 \pm 0.04	269.2 \pm 55.2	-259.7 \pm 53.1
α 1 Δ 6a	4	0.25 \pm 0.2	-0.05 \pm 0.3	758.1 \pm 248.6	-689.9 \pm 222.2
α 1 Δ 6b	5	0.3 \pm 0.1	-0.2 \pm 0.02	1402.9 \pm 324.0	-1334.9 \pm 325.2
α 1 Δ 12	6	35.6 \pm 13.9	-3.8 \pm 1.7	0.8 \pm 0.4	-1.7 \pm 0.7
α 2 + 5	4	1.2 \pm 0.6	-0.1 \pm 0.1	972.8 \pm 313.1	-815.4 \pm 275.9
α 2 + 4	6	1.1 \pm 0.4	-0.3 \pm 0.2	931.6 \pm 153.1	-805.9 \pm 148.6
α 2 + 3	5	7.8 \pm 2.0	-1.3 \pm 0.4	1293.6 \pm 230.3	-1151.8 \pm 202.9
α 2 + 2	4	1.2 \pm 0.6	-0.1 \pm 0.2	1409.4 \pm 236.2	-1262.9 \pm 235.9
α 2 + 1	4	45.2 \pm 18.6	-2.2 \pm 0.6	645.5 \pm 155.5	-595.5 \pm 136.4

Note: Mean delta current increases of number (n) of measured cells upon application of pregnenolone sulphate (PS; 40 μ M) or clotrimazole (Clt; 10 μ M) are shown for TRPM3 α 1, TRPM3 α 2 and all designed mutants at \pm 80 mV. Constructs resembling the activation profile of TRPM3 α 1 are coloured in white and constructs resembling the activation profile of TRPM3 α 2 are colored in yellow. Constructs that show a mixed phenotype are indicated in grey.

unable to block the clotrimazole-induced currents in the TRPM3 α 2 +1 mutant channel (Figure 7j).

Altogether, these results suggest that differences in pharmacology between the long and short pore loop variants of TRPM3 α are mainly determined by the length of the pore loop. Moreover, the potency of TRPM3 blockers is strongly dependent on the ligand that is used to activate the channel.

4 | DISCUSSION AND CONCLUSIONS

In earlier work, several isoforms of the TRPM3 channel have been described (Frühwald et al., 2012; Lee et al., 2003; Oberwinkler et al., 2005), but the expression profile, pharmacology and physiological roles of the different channel variants have remained largely unknown. Here, we focused on alternative splicing at the junction between exon 24 and exon 25, which gives rise to TRPM3 variants with either a short or a long pore loop. By analysing RNA-sequencing data in different murine tissues, we found that the relative expression of the short versus long pore variants is tissue dependent. In DRG neurons, where TRPM3 activity has been extensively studied, only reads corresponding to the short pore variants were detected. However, substantial levels of reads corresponding to the long pore loop were found in other tissues, for instance the retina and in CNS areas such as the dentate gyrus and cerebellum.

Next, the functional consequences of alternative splicing were assessed. TRPM3 α 1 could not be activated by stimulation with pregnenolone sulphate and nifedipine, both well-characterized ligands of the short pore loop TRPM3 α variants. In contrast, clotrimazole was

identified, which by itself does not activate TRPM3 α 2 but potentiates pregnenolone sulphate-induced responses, as a potent agonist of TRPM3 α 1. A plausible explanation for the strong inward currents after stimulation by clotrimazole in TRPM3 α 1 expressing cells is the opening of the non-canonical pore of TRPM3. However, another possibility could be that the insertion of 12 additional residues in the pore region of TRPM3 α 1 strongly alters the properties of the central pore or modifies the gating mechanism of the channel.

The synthetic peptide CIM0216, currently the most potent agonist of TRPM3 α 2 described, was found to be a modest TRPM3 α 1 agonist, inducing outwardly rectifying currents and small but sizeable calcium signals in microfluorimetric experiments. The relatively small amplitudes of the calcium response to CIM0216 can be explained by a combination of small inward currents and the low calcium permeability of TRPM3 α 1 ($P_{Ca^{2+}}/P_{Na^{+}} = 0.7$) (Oberwinkler et al., 2005).

Next, this study reveals the importance of the length of the pore loop for the pharmacology of the TRPM3 channel. Pregnenolone sulphate and nifedipine are both well-described channel agonists for the short pore loop TRPM3 α variants, but none of these stimuli could activate TRPM3 α 1. In addition, TRPM3 α 2 inhibitors like isosakuranetin, diclofenac, primidone and the $G_{\beta\gamma}$ subunit of GPCR showed significantly reduced blocking potencies on the clotrimazole-induced TRPM3 α 1 currents. A plausible mechanism could be that the interaction site for these TRPM3 ligands is located in the pore loop area and that the insertion of extra amino residues in this area alters their ligand affinity. This hypothesis may explain why pregnenolone sulphate responses are lost as soon as two or more amino residues were inserted in the pore loop of TRPM3 α 2. In line herewith, outside-out patch clamp studies have revealed that the

pregnenolone sulphate interaction site is located at the extracellular side of the plasma membrane (Wagner et al., 2008). Moreover, a potential pregnenolone sulphate-interaction motive Gln-Ile-Asp (or QID) was identified in the **NMDA receptor** that is critical for both pregnenolone sulphate enhancement and proton sensitivity (Jang, Mierke, Russek, & Farb, 2004). Interestingly, a similar QID motive is present in the pore-forming loop of both TRPM3 α pore variants. Since the 12 additional amino acid residues of the long pore loop variant are inserted directly after the QID motive (Figure 6), this extension may indeed result in a disturbed interaction between pregnenolone sulphate and the pore loop. However, since the action of several antagonists on TRPM3 α 1 depended on the activating ligand (i.e. strong block of CIM0216-induced currents vs. weak block of clotrimazole-induced currents), the pore loop length does not seem to affect interaction site for these antagonists. In line with these results, the TRPM3 α 2 +1 mutant showed full current inhibition to the tested TRPM3 antagonists when activated with pregnenolone sulphate, while only small inhibition was recorded when activated by clotrimazole. A second and arguably more plausible explanation is that the length of the pore loop causes a structural change in the protein that substantially alters the gating mechanism of the channel. This hypothesis can be supported by firstly the altered pharmacology for TRPM3 α 1 to TRPM3 agonists (pregnenolone sulphate and nifedipine), antagonists (isosakuranetin, primidone, diclofenac and the G $\beta\gamma$ subunit) and the modulator clotrimazole. Secondly, the finding that the potency of TRPM3 blockers towards TRPM3 α 1 is strongly dependent on the agonist that is used to induce channel activation. In contrast, similar potencies were described in TRPM3 α 2 cells for isosakuranetin (5 μ M) to induce a full block of the channel activity after activation by pregnenolone sulphate and CIM0216 (Straub et al., 2013).

Altogether, this study illustrates the distinct pharmacological profile of the long and short pore loop TRPM3 α variants and the importance of the length of the pore-forming loop between S5 and S6. This structural difference alters the gating properties of the pore loop variants, resulting in two distinct ion channels with different biophysical characteristics.

Using immunoprecipitation experiments, we demonstrated that TRPM3 α 1 and TRPM3 α 2 can physically interact, which may point at the formation of heteromultimeric channel complexes. Functionally, co-expression of increasing levels of TRPM3 α 1 with TRPM3 α 2 led to a gradual decrease of pregnenolone sulphate-induced calcium responses, which suggests that TRPM3 α 1 could act as a negative regulator of the pregnenolone sulphate-induced calcium influx in tissues co-expressing both splice variants, such as the eye or specific brain regions. However, additional experiments are required to provide further evidence for the formation and physiological roles of TRPM3 α 1/ α 2 heteromultimeric channel complexes.

Expression of TRPM3 is identified in the peripheral nervous system where the channel has been introduced as a potential target for pain relief. TRPM3-deficient mice have a partial deficit in acute heat sensing and fail to develop inflammatory thermal hyperalgesia (Vriens et al., 2011). Preclinical studies have shown that inhibition of

the channel attenuates acute heat pain as well as thermal and mechanical hypersensitivity in the context of inflammation or nerve injury (Jia, Zhang, & Yu, 2017; Krugel et al., 2017) and indicated TRPM3 as a potential target for the development of novel analgesics. Since the expression of TRPM3 α pore variants in sensory DRG neurons is restricted to the short pore variants, the screening of novel TRPM3 inhibitors as analgesics is advised be done on these isoforms. Contrarily, in tissues co-expressing both TRPM3 α pore variants, such as the retina and the cerebellum, it is possible that the activation by pregnenolone sulphate or the blocking potency of an inhibitor is reduced by the interference of both splice variants, as our results showed that alternative splicing in the pore-forming region of TRPM3 defines the channel's pharmacological properties.

ACKNOWLEDGEMENTS

We thank all the members of the Laboratory of Ion Channel Research and the Laboratory of Endometrium, Endometriosis and Reproduction at the KU Leuven for their helpful discussions and comments. This project has received funding from the Belgian Federal Government (IUAP P7/13 to T.V.), the Research Foundation–Flanders (G.0565.07 and G.0825.11 to T.V. and J.V.; G.084515N and G.0B1819N to J.V.), the Research Council of the KU Leuven (C1-TRPLe to T.V.), the Queen Elisabeth Medical Foundation for Neurosciences (to T.V.), the Belgian Foundation Against Cancer (to J.V. and T.V.) and the Saarland University (HOMFOR) (to S.E.P.). The manuscript was published with support of the University Foundation from Belgium (WA-0292 to K.H.). K.H. is a “postdoctoral fellow” of the Research Foundation–Flanders, Belgium and a research trainee of the Michael Smith Foundation for Health Research/Vancouver Coastal Health Research Institute/VGH and UBC Hospital Foundation.

AUTHOR CONTRIBUTIONS

This work was performed in the Laboratory of Ion Channel Research at the KU Leuven and at the Centre for Brain Health at the University of British Columbia. K.H., T.V. and J.V. designed the work; K.H., J.V., A.C.N.F., V.D.A., A.J., A.S and J.P. acquired and analysed the data; K.H., T.V. and J.V. interpreted the data; K.H., V.D.A., S.E.P., Y.T.W., T.V. and J.V. drafted the work; and S.E.P., Y.T.W., T.V. and J.V. revised the work critically. All listed authors approved the final version of the manuscript and agree to be accountable for all aspects of the work in ensuring that questions related to the accuracy or integrity of any part of the work are appropriately investigated and resolved. All above listed authors qualify for authorship and all persons qualifying for authorship are listed above.

CONFLICT OF INTEREST

J.V. and T.V. are co-inventors on patents entitled “treatment of pain” derived from WO2012149614.

DECLARATION OF TRANSPARENCY AND SCIENTIFIC RIGOUR

This Declaration acknowledges that this paper adheres to the principles for transparent reporting and scientific rigour of preclinical

research as stated in the *BJP* guidelines for [Design & Analysis, Immunoblotting and Immunochemistry](#) and as recommended by funding agencies, publishers and other organizations engaged with supporting research.

ORCID

Katharina Held  <https://orcid.org/0000-0002-1727-9517>

Thomas Voets  <https://orcid.org/0000-0001-5526-5821>

Joris Vriens  <https://orcid.org/0000-0002-2502-0409>

REFERENCES

- Alexander, S. P. H., Mathie, A., Peters, J. A., Veale, E. L., Striessnig, J., Kelly, E., ... Collaborators, C. (2019). THE CONCISE GUIDE TO PHARMACOLOGY 2019/20: Ion channels. *British Journal of Pharmacology*, 176(Suppl 1), S142–S228.
- Alexander, S. P. H., Roberts, R. E., Broughton, B. R. S., Sobey, C. G., George, C. H., Stanford, S. C., ... Ahluwalia, A. (2018). Goals and practicalities of immunoblotting and immunohistochemistry: A guide for submission to the *British Journal of Pharmacology*. *British Journal of Pharmacology*, 175, 407–411. <https://doi.org/10.1111/bph.14112>
- Badheka, D., Yudin, Y., Borbiro, I., Hartle, C. M., Yazici, A., Mirshahi, T., & Rohacs, T. (2017). Inhibition of transient receptor potential melastatin 3 ion channels by G-protein $\beta\gamma$ subunits. *eLife*, 6. <https://doi.org/10.7554/eLife.26147>
- Cembrowski, M. S., Wang, L., Sugino, K., Shields, B. C., & Spruston, N. (2016). Hipposeq: A comprehensive RNA-seq database of gene expression in hippocampal principal neurons. *eLife*, 5, e14997.
- Curtis, M. J., Alexander, S., Cirino, G., Docherty, J. R., George, C. H., Giembycz, M. A., ... Ahluwalia, A. (2018). Experimental design and analysis and their reporting II: Updated and simplified guidance for authors and peer reviewers. *British Journal of Pharmacology*, 175, 987–993. <https://doi.org/10.1111/bph.14153>
- Curtis, M. J., Bond, R. A., Spina, D., Ahluwalia, A., Alexander, S. P., Giembycz, M. A., ... McGrath, J. C. (2015). Experimental design and analysis and their reporting: New guidance for publication in *BJP*. *British Journal of Pharmacology*, 172, 3461–3471. <https://doi.org/10.1111/bph.12856>
- De Clercq, K., Van den Eynde, C., Hennes, A., Van Bree, R., Voets, T., & Vriens, J. (2017). The functional expression of transient receptor potential channels in the mouse endometrium. *Human Reproduction*, 32, 615–630. <https://doi.org/10.1093/humrep/dew344>
- Dembla, S., Behrendt, M., Mohr, F., Goecke, C., Sondermann, J., Schneider, F. M., ... Oberwinkler, J. (2017). Anti-nociceptive action of peripheral mu-opioid receptors by G-beta-gamma protein-mediated inhibition of TRPM3 channels. *eLife*, 6.
- Dobin, A., Davis, C. A., Schlesinger, F., Drenkow, J., Zaleski, C., Jha, S., ... Gingeras, T. R. (2013). STAR: Ultrafast universal RNA-seq aligner. *Bioinformatics*, 29, 15–21. <https://doi.org/10.1093/bioinformatics/bts635>
- Frühwald, J., Camacho Londono, J., Dembla, S., Mannebach, S., Lis, A., Drews, A., ... Philipp, S. E. (2012). Alternative splicing of a protein domain indispensable for function of transient receptor potential melastatin 3 (TRPM3) ion channels. *The Journal of Biological Chemistry*, 287, 36663–36672. <https://doi.org/10.1074/jbc.M112.396663>
- Grimm, C., Kraft, R., Sauerbruch, S., Schultz, G., & Harteneck, C. (2003). Molecular and functional characterization of the melastatin-related cation channel TRPM3. *The Journal of Biological Chemistry*, 278, 21493–21501. <https://doi.org/10.1074/jbc.M300945200>
- Grynkiewicz, G., Poenie, M., & Tsien, R. Y. (1985). A new generation of Ca^{2+} indicators with greatly improved fluorescence properties. *The Journal of Biological Chemistry*, 260, 3440–3450.
- Held, K., Gruss, F., Aloï, V. D., Janssens, A., Ulens, C., Voets, T., & Vriens, J. (2018). Mutations in the voltage-sensing domain affect the alternative ion permeation pathway in the TRPM3 channel. *The Journal of Physiology*, 596, 2413–2432. <https://doi.org/10.1113/JP274124>
- Held, K., Kichko, T., De Clercq, K., Klaassen, H., Van Bree, R., Vanherck, J. C., ... Vriens, J. (2015). Activation of TRPM3 by a potent synthetic ligand reveals a role in peptide release. *Proceedings of the National Academy of Sciences of the United States of America*, 112, E1363–E1372. <https://doi.org/10.1073/pnas.1419845112>
- Jang, M. K., Mierke, D. F., Russek, S. J., & Farb, D. H. (2004). A steroid modulatory domain on NR2B controls N-methyl-D-aspartate receptor proton sensitivity. *Proceedings of the National Academy of Sciences of the United States of America*, 101, 8198–8203. <https://doi.org/10.1073/pnas.0401838101>
- Jia, S., Zhang, Y., & Yu, J. (2017). Antinociceptive effects of isosakuranetin in a rat model of peripheral neuropathy. *Pharmacology*, 100, 201–207. <https://doi.org/10.1159/000478986>
- Krugel, U., Straub, I., Beckmann, H., & Schaefer, M. (2017). Primidone inhibits TRPM3 and attenuates thermal nociception in vivo. *Pain*, 158, 856–867. <https://doi.org/10.1097/j.pain.0000000000000846>
- Lee, N., Chen, J., Sun, L., Wu, S., Gray, K. R., Rich, A., ... Blonar, M. A. (2003). Expression and characterization of human transient receptor potential melastatin 3 (hTRPM3). *The Journal of Biological Chemistry*, 278, 20890–20897. <https://doi.org/10.1074/jbc.M211232200>
- Lu, G., Henderson, D., Liu, L., Reinhart, P. H., & Simon, S. A. (2005). TRPV1b, a functional human vanilloid receptor splice variant. *Molecular Pharmacology*, 67, 1119–1127. <https://doi.org/10.1124/mol.104.009852>
- Lun, M. P., Johnson, M. B., Broadbelt, K. G., Watanabe, M., Kang, Y. J., Chau, K. F., ... Lehtinen, M. K. (2015). Spatially heterogeneous choroid plexus transcriptomes encode positional identity and contribute to regional CSF production. *J Neurosci*, 35, 4903–4916.
- Oberwinkler, J., Lis, A., Giehl, K. M., Flockerzi, V., & Philipp, S. E. (2005). Alternative splicing switches the divalent cation selectivity of TRPM3 channels. *The Journal of Biological Chemistry*, 280, 22540–22548. <https://doi.org/10.1074/jbc.M503092200>
- Oberwinkler, J., & Philipp, S. E. (2014). TRPM3. *Handbook of Experimental Pharmacology*, 222, 427–459. https://doi.org/10.1007/978-3-642-54215-2_17
- Quallo, T., Alkhatib, O., Gentry, C., Andersson, D. A., & Bevan, S. (2017). G protein $\beta\gamma$ subunits inhibit TRPM3 ion channels in sensory neurons. *eLife*, 6. <https://doi.org/10.7554/eLife.26138>
- Robinson, J. T., Thorvaldsdottir, H., Winckler, W., Guttman, M., Lander, E. S., Getz, G., & Mesirov, J. P. (2011). Integrative Genomics Viewer. *Nature Biotechnology*, 29, 24–26. <https://doi.org/10.1038/nbt.1754>
- Rubil, S., & Thiel, G. (2017). Activation of gene transcription via CIM0216, a synthetic ligand of transient receptor potential melastatin-3 (TRPM3) channels. *Channels (Austin, Tex.)*, 11, 79–83. <https://doi.org/10.1080/19336950.2016.1207026>
- Sabnis, A. S., Shadid, M., Yost, G. S., & Reilly, C. A. (2008). Human lung epithelial cells express a functional cold-sensing TRPM8 variant. *American Journal of Respiratory Cell and Molecular Biology*, 39, 466–474. <https://doi.org/10.1165/rcmb.2007-0440OC>
- Straub, I., Krugel, U., Mohr, F., Teichert, J., Rizun, O., Konrad, M., ... Schaefer, M. (2013). Flavanones that selectively inhibit TRPM3 attenuate thermal nociception in vivo. *Molecular Pharmacology*, 84, 736–750. <https://doi.org/10.1124/mol.113.086843>
- Suzuki, H., Sasaki, E., Nakagawa, A., Muraki, Y., Hatano, N., & Muraki, K. (2016). Diclofenac, a nonsteroidal anti-inflammatory drug, is an antagonist of human TRPM3 isoforms. *Pharmacology Research & Perspectives*, 4, e00232. <https://doi.org/10.1002/prp2.232>
- The ENCODE Project Consortium. (2012). An integrated encyclopedia of DNA elements in the human genome. *Nature*, 489, 57–74.
- Vandewauw, I., De Clercq, K., Mulier, M., Held, K., Pinto, S., Van Ranst, N., ... Voets, T. (2018). A TRP channel trio mediates acute noxious heat sensing. *Nature*, 555, 662–666.

- Vriens, J., Held, K., Janssens, A., Toth, B. I., Kerselaers, S., Nilius, B., ... Voets, T. (2014). Opening of an alternative ion permeation pathway in a nociceptor TRP channel. *Nature Chemical Biology*, 10, 188–195. <https://doi.org/10.1038/nchembio.1428>
- Vriens, J., Owsianik, G., Hofmann, T., Philipp, S. E., Stab, J., Chen, X., ... Voets, T. (2011). TRPM3 is a nociceptor channel involved in the detection of noxious heat. *Neuron*, 70, 482–494. <https://doi.org/10.1016/j.neuron.2011.02.051>
- Vriens, J., Owsianik, G., Janssens, A., Voets, T., & Nilius, B. (2007). Determinants of 4 alpha-phorbol sensitivity in transmembrane domains 3 and 4 of the cation channel TRPV4. *The Journal of Biological Chemistry*, 282, 12796–12803. <https://doi.org/10.1074/jbc.M610485200>
- Wagner, T. F., Loch, S., Lambert, S., Straub, I., Mannebach, S., Mathar, I., ... Oberwinkler, J. (2008). Transient receptor potential M3 channels are ionotropic steroid receptors in pancreatic beta cells. *Nature Cell Biology*, 10, 1421–1430. <https://doi.org/10.1038/ncb1801>
- Wang, J., Geisert, E. E., & Struebing, F. L. (2019). RNA-sequencing profiling of the retina in C57BL/6J and DBA/2J mice: Enhancing the retinal microarray data sets from GeneNetwork. *Mol Vis*, 25, 345–358.
- Zhou, Y., Suzuki, Y., Uchida, K., & Tominaga, M. (2013). Identification of a splice variant of mouse TRPA1 that regulates TRPA1 activity. *Nature Communications*, 4, 2399. <https://doi.org/10.1038/ncomms3399>
- Zhou, Z., & Neher, E. (1993). Mobile and immobile calcium buffers in bovine adrenal chromaffin cells. *The Journal of Physiology*, 469, 245–273. <https://doi.org/10.1113/jphysiol.1993.sp019813>

SUPPORTING INFORMATION

Additional supporting information may be found online in the Supporting Information section at the end of this article.

How to cite this article: Held K, Aloï VD, Freitas ACN, et al. Pharmacological properties of TRPM3 isoforms are determined by the length of the pore loop. *Br J Pharmacol*. 2020;1–16. <https://doi.org/10.1111/bph.15223>